Supplemental material

Kalinski et al., https://doi.org/10.1083/jcb.201702187

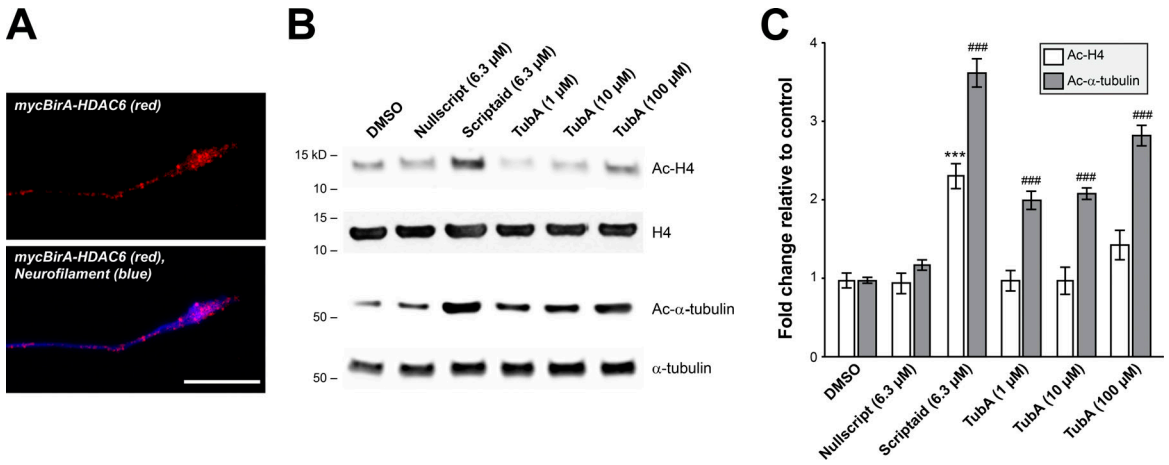

Figure S1. **TubA increases Ac-α-tubulin levels without affecting histone acetylation. (A)** Representative confocal projection images (XYZ) of terminal axons of DRGs expressing myc-tagged HDAC6 are shown, with anti-Myc (FITC) and NF (Cy3) as indicated. Images were cropped, pseudocolored, and merged using ImageJ (scale bar = 10 µm). **(B and C)** Representative immunoblots for acetylated histone H4 (Ac-H4), total histone H4 (H4), Ac-α-tubulin, and total α-tubulin signals for DRGs exposed to vehicle (control), pan-HDAC inhibitor Scriptaid, Nullscript, or HDAC6 inhibitor Tubastatin A (TubA) at indicated concentrations for 12 h are shown in B. C shows quantification of immunoblots across three separate culture experiments as average relative to DMSO ± SEM (n = 3; ***, $P \leq 0.005$; ###, $P \leq 0.005$ for Ac-H4 and Ac-α-tubulin vs. DMSO by two-way ANOVA with Tukey post hoc).

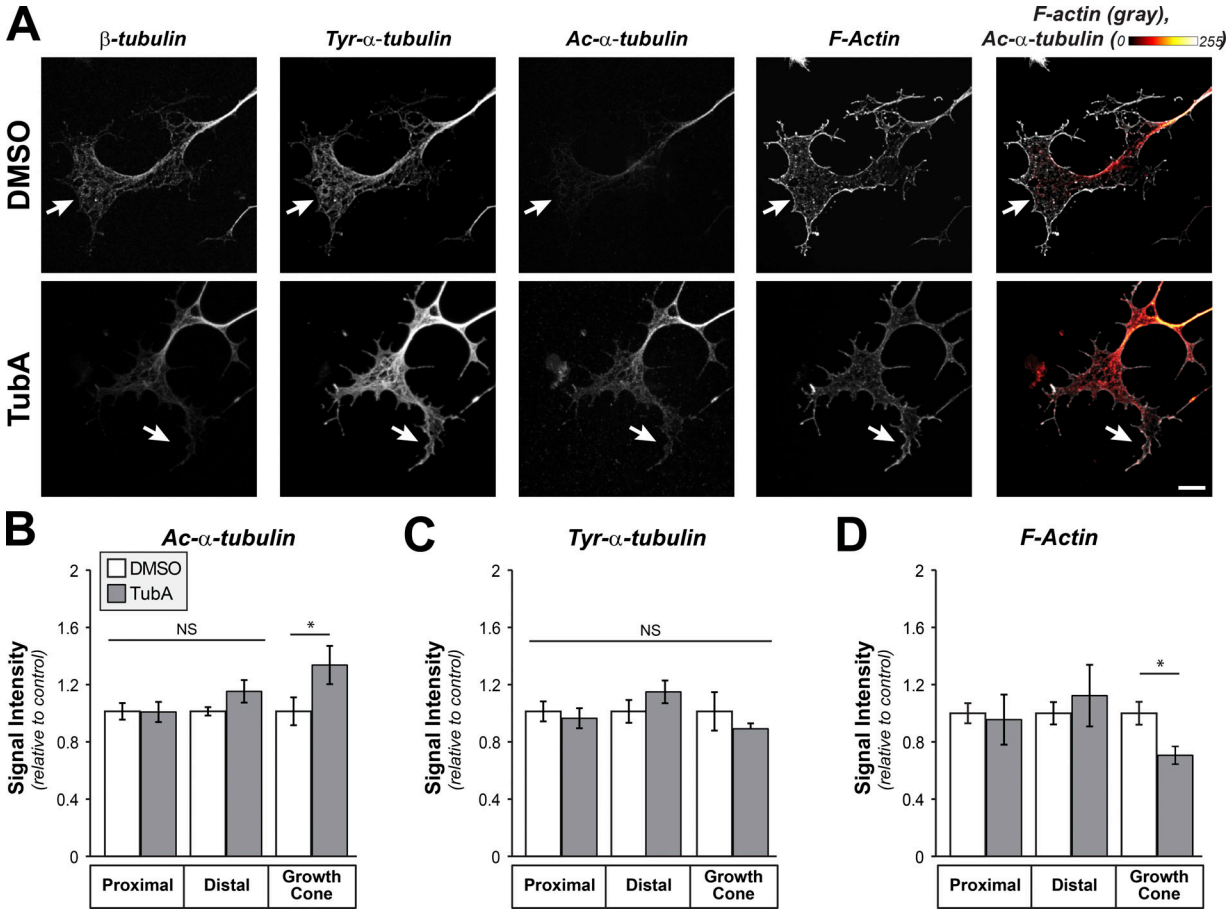

Figure S2. **Inhibition of HDAC6 triggers rapid increase in axonal acetylated α-tubulin. (A)** Representative confocal projection images (XYZ) are shown for β-tubulin (FITC), tyrosyl-α-tubulin (Tyr-α-tubulin; Cy5), Ac-α-tubulin (Alexa Fluor 405), and phalloidin (F-actin; Alexa Fluor 555) are shown as indicated for DRG neurons cultured on laminin and exposed with vehicle control (DMSO) or 10 µM TubA for 1 h. Exposure times and gain matched for all image pairs; images were median filtered using LAS-X software (matched parameters for all images). Far right panel shows merged signals for Ac-α-tubulin (indicated spectrum) and F-actin (gray). Arrows indicate position of growth cone across image sets (scale bar = 10 µm). **(B–D)** Quantification of signals for Ac-α-tubulin (B), Tyr-α-tubulin (C), and F-actin (D) in indicated regions of axon are shown average fold-change relative to vehicle control ± SEM. Exposure-matched images were used for quantification. Growth cone signals for Ac-α-tubulin are increased and for F-actin are decreased after HDAC6 inhibition ($n \geq 25$ neurons from three culture preparations; *, $P \leq 0.05$ and NS by one-way ANOVA with Bonferroni post hoc analysis).

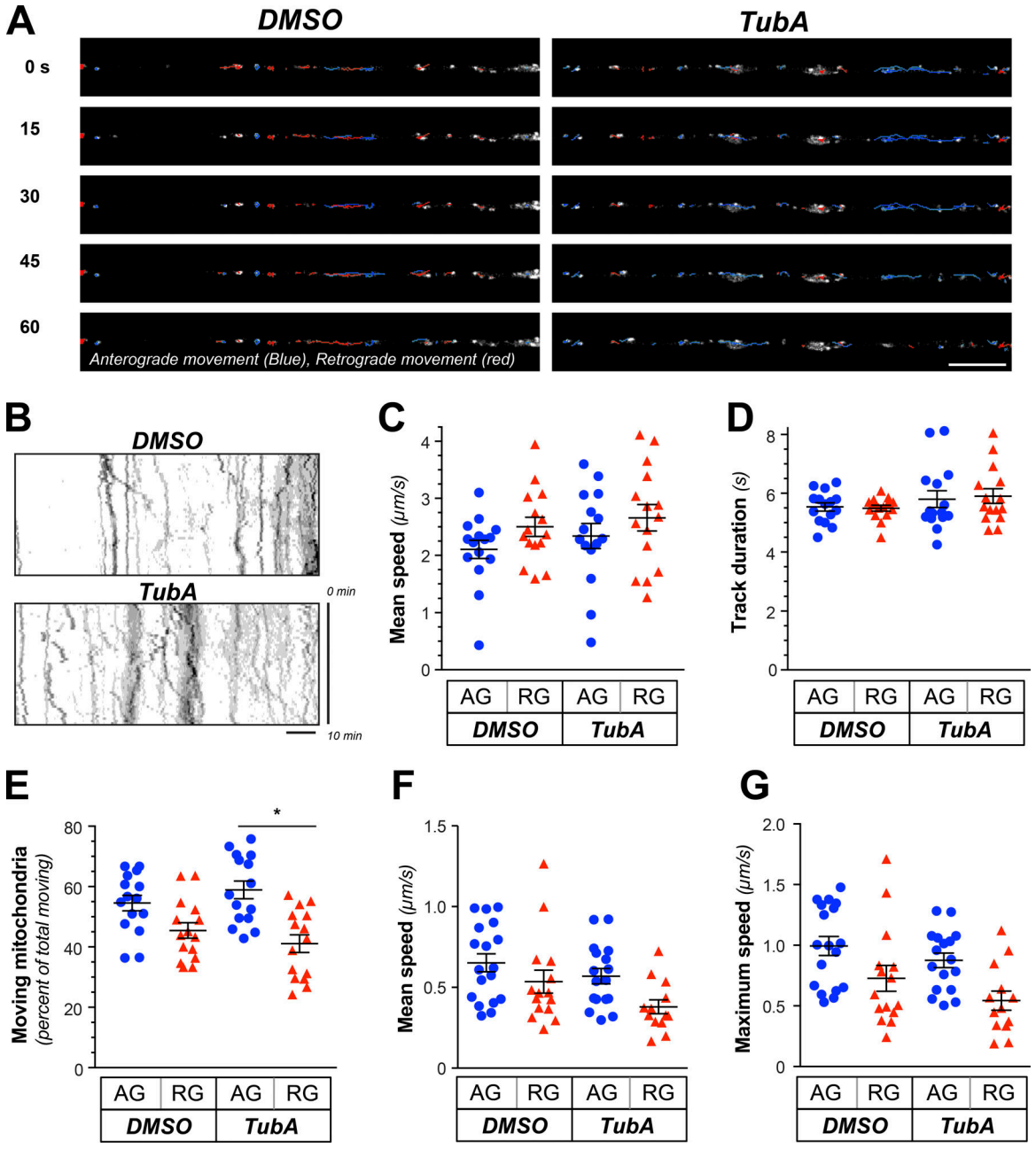

Figure S3. **HDAC6 inhibition causes a net shift in mitochondrial transport toward anterograde movement. (A)** Representative time-lapse image sequence of axon shafts for dissociated DRG cultured on laminin and stained with MitoTracker Green (gray) after 1-h treatment with 10 µM TubA or vehicle control (DMSO). The images are oriented with proximal on left and distal on right based on positioning of neuronal cell body and distal axon/growth cone. Difference tracker plugin for ImageJ was used for track tracking, with blue traces indicating anterograde tracks and red traces indicating retrograde tracks between time points (distal progresses from left to right); parenthetic values indicate durations for time tracks (scale bar = 10 µm; 100×/1.4 NA objective used). **(B)** Representative kymographs from 10-min image sequences as in A for DMSO-treated vs. TubA-treated cultures as in A. Proximal is on left and distal on right. Horizontal scale is distance and vertical scale is time as indicated. **(C–E)** Velocity (C), track duration (D), and percentage of motile mitochondria (E) in axon shaft over 10-min imaging sequences are shown for DRG cultures treated with 10 µM TubA for 1 h as average values ± SEM. There are no significant changes in velocity or track durations. There was also no significant change in total numbers of motile mitochondria (motile mitochondria average of 109.5 ± 16.6 in DMSO and 136.5 ± 22.1 in TubA and static mitochondria of 202.5 ± 27.6 in DMSO and 237.5 ± 29.5 in TubA; $n \geq 13$ axons across at least three culture preparations; *, $P \leq 0.05$ by ANOVA with Holm–Sidak's multiple comparisons test). **(F and G)** Mean and maximum speed for in vivo axonal mitochondrial kinetics analyses from Fig. 2 are shown as average values ± SEM. No statistically significant differences were detected by ANOVA with Holm–Sidak's multiple comparisons test ($n \geq 13$ axons tracked over four animals).

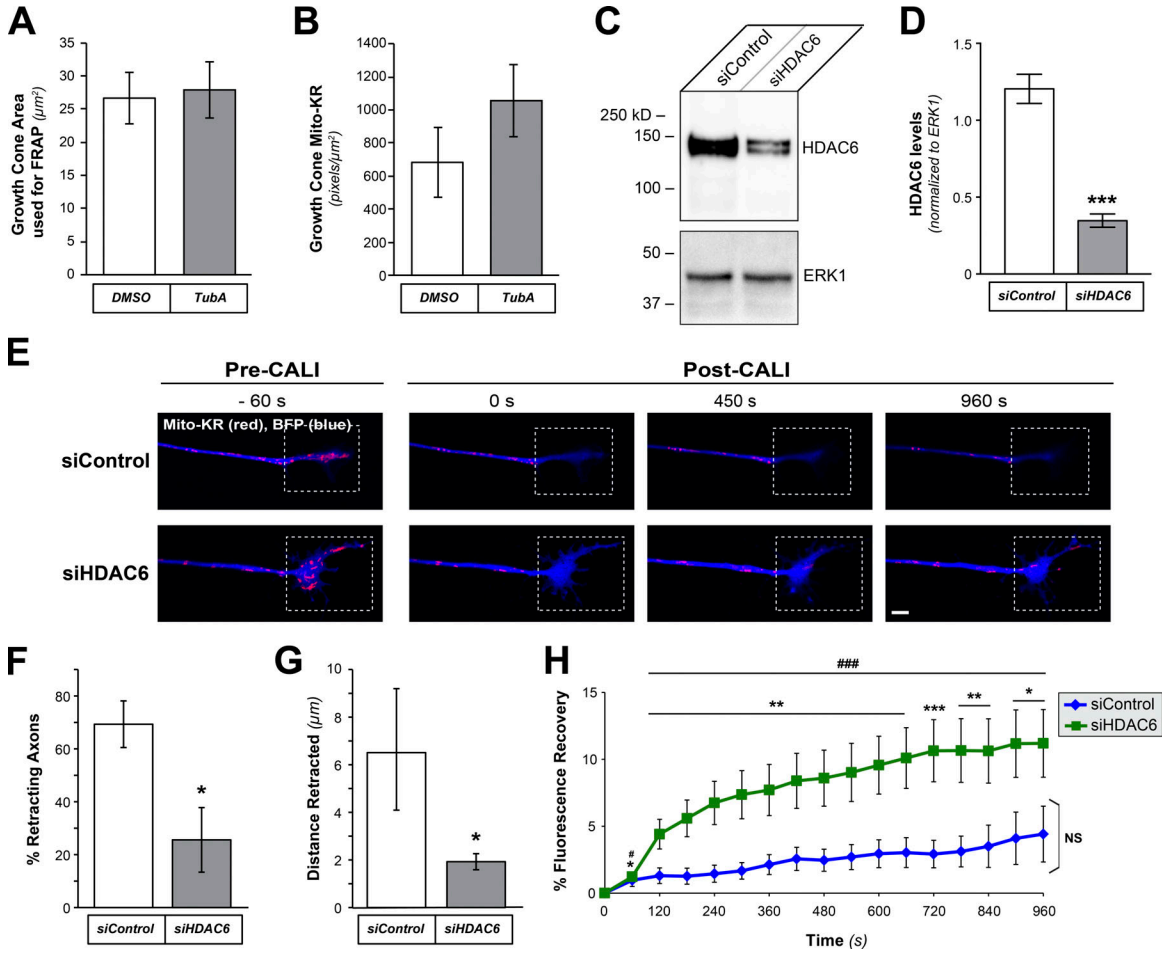

Figure S4. **Growth cones of HDAC6-depleted DRG neurons are protected from collapse after mitochondrial ablation. (A and B)** Pre-CALI sequence growth cone area and Mito-KR signal intensities for axons analyzed in Fig. 3 are shown as average ± SEM (NS by Student's *t* test using Wilcoxon matched-pairs signed rank test). **(C and D)** Protein lysates from DRGs transfected with control versus HDAC6 siRNAs (siControl and siHDAC6, respectively) show clear depletion of HDAC6 protein by immunoblotting (C). Average band intensity normalized to ERK1 across multiple transfections ± SEM shows significant depletion of HDAC6 protein (D; $n = 3$; ***, $P \le 0.005$ by Student's *t* test). **(E)** Representative time-lapse images from CALI sequence are shown for DRGs transfected with control or HDAC6 siRNAs (siControl and siHDAC6, respectively) and cultured on laminin as in Fig. 4. BFP is shown in blue to mark the axons, and Mito-KR is shown in red. Box represents ROI for distal axon and growth cone that was subjected to photoactivation of Mito-KR to ablate mitochondria. ImageJ was used for image cropping, pseudocoloring, channel merging, and brightness/contrast adjustment (equivalent parameter used across image sequences; scale bar = 10 µm; 63×/1.4 NA objective used). **(F and G)** Quantifications of axon retraction (B) and distance that individual axons retracted (C) from image sequences as in A are shown as average ± SEM ($n \ge 20$ across three culture preparations; *, $P \le 0.05$ by one-way ANOVA with Bonferroni post hoc). **(H)** Recovery of Mito-KR fluorescence in photoactivated ROI from image sequences as in A is shown as average normalized percentage recovery ± SEM ($n \ge 20$ axons from three independent experiments; *, $P \le 0.05$; **, $P \le 0.01$; ***, $P \le 0.005$; NS vehicle time points vs. $t = 0$ s; ###, $P \le 0.001$ for siHDAC6 vs. siControl by one-way ANOVA with Bonferroni post hoc).

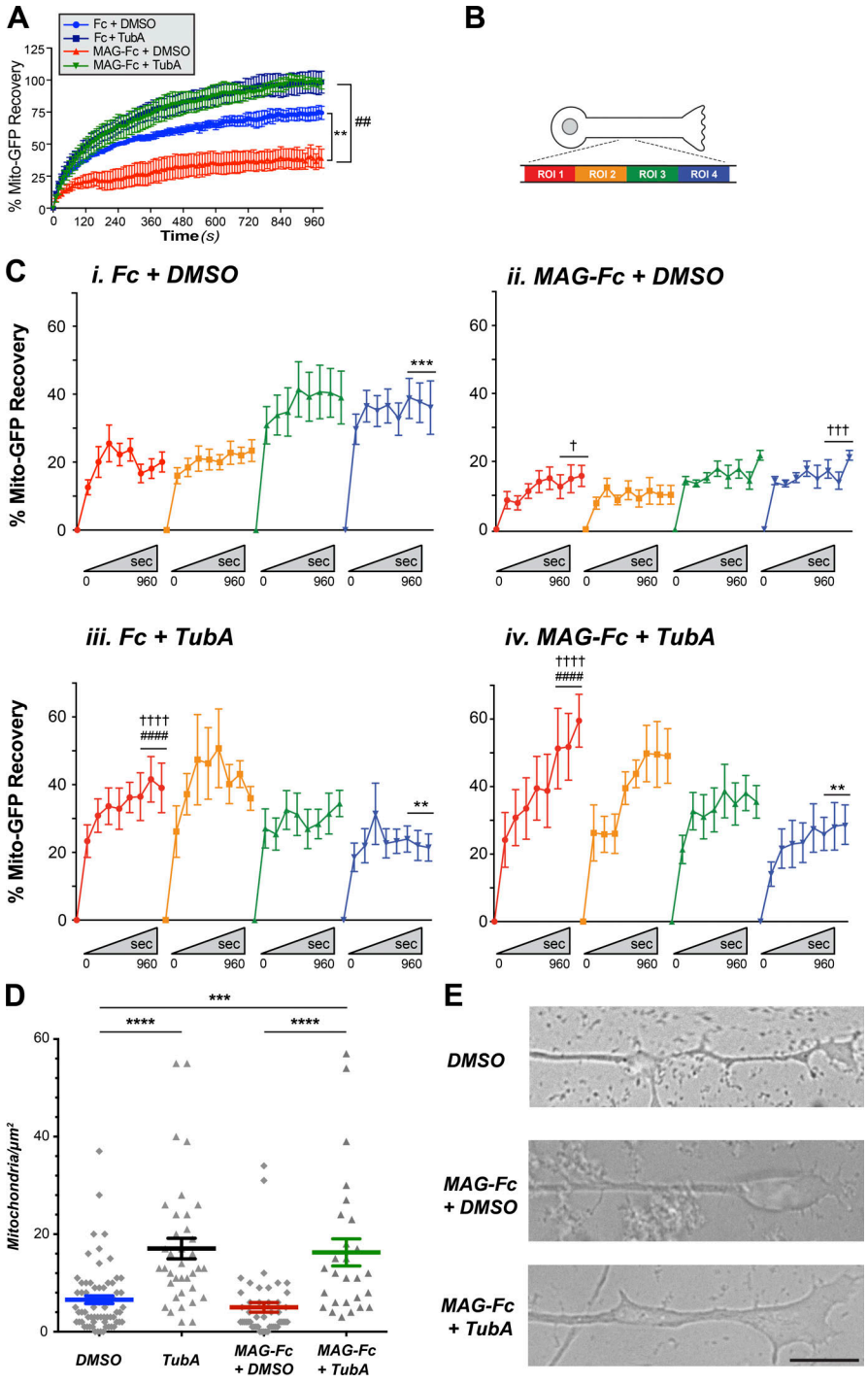

Figure S5. **MAG attenuates mitochondrial transport through axon-intrinsic mechanisms. (A)** Recovery curves for FRAP analyses of Mito-GFP fluorescence in distal axons of DRGs cultured on laminin and treated with bath-applied Fc versus MAG-Fc as reported in Fig. 4 B are shown as normalized percentage recovery ± SEM ($n \geq 12$ axons over four culture preparations; **, $P \leq 0.05$ vs. Fc-control; ##, $P \leq 0.01$ vs. MAG + vehicle by two-way ANOVA with Tukey post hoc). **(B)** Schematic of ROIs analyzed for recovery in B after photobleaching axon shaft. **(C)** FRAP analyses for Mito-GFP recovery in axon shafts of DRGs cultured on laminin and treated with bath-applied Fc versus MAG-Fc as in A are shown as average of normalized percentage recovery ± SEM in individual 10-µm bins within the bleached ROI across the 960-s recovery sequence as in A. Proximal bins are on the left and distal bins on the right of each graph as indicated in the schematic ($n \geq 25$ axons over four culture preparations; symbols are: * for intra-graph comparison of ROI 4 vs. ROI 1; † for sequence ROIs indicated vs. corresponding ROI in Fc + DMSO; and # for sequence ROIs indicated vs. corresponding ROI in MAG + DMSO where one symbol = $P \leq 0.05$, two symbols = $P \leq 0.01$, three symbols = $P \leq 0.005$, and four symbols = $P \leq 0.001$ for pooled time points by Kolmogorov–Smirnov *t* test). **(D)** Quantification of mitochondria in distal axons at 4 h after bath application of 25 µg/ml MAG-Fc to axonal compartment in microfluidic cultures is shown as average. Horizontal lines indicate mean, with error bars showing SEM ($n \geq 30$ axons assessed over two separate cultures; ***, $P \leq 0.005$; ****, $P \leq 0.0001$ by one-way ANOVA with Bonferroni post hoc). **(E)** Representative bright-field images of distal axons of cultures treated as in A are shown. MAG-Fc triggers growth cone retraction that is prevented by inhibition of HDAC6 with 10 µM TubA. ImageJ was used to crop images for highlighting growth cones (scale bar = 10 µm).

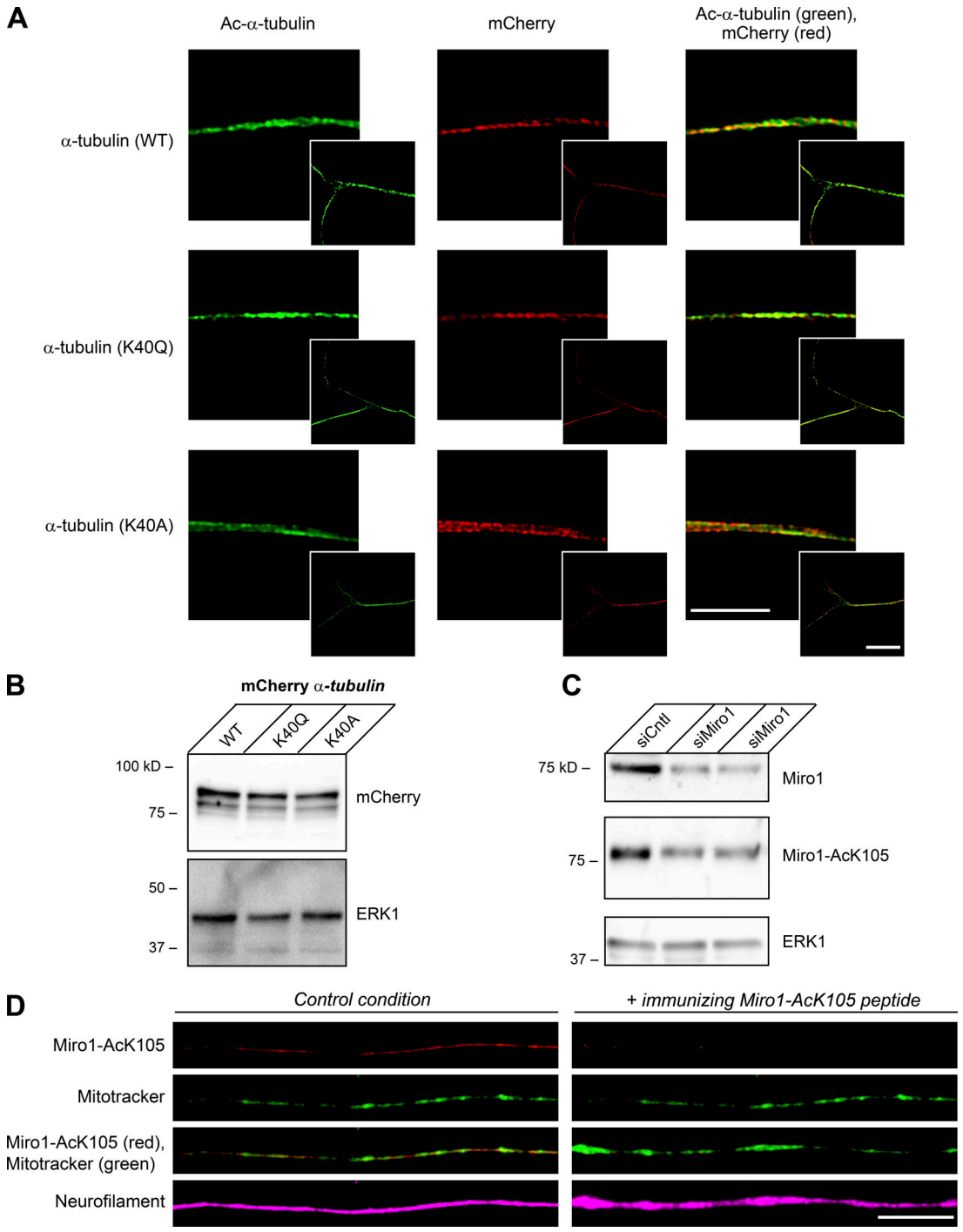

Figure S6. **Acetylation of Miro1 in DRG neurons. (A)** Representative confocal projection images (XYZ) of axon shafts for cultured DRG neurons transfected with WT, Ac-mimetic (K40Q), or nonacetylatable (K40A) mCherry-α-tubulin proteins stained with antibodies for Ac-α-tubulin (FITC) are shown. Inset panels show low-magnification and main panels show high-magnification XYZ projections. Images were after processed using Lightning software for deconvolution and LAS-X software for median filtering (matched parameters across image sets); ImageJ was used for pseudocoloring and channel merging (scale bars = 5 µm for large panel and 20 µm for inset panels; 100×/1.4 NA objective used). **(B)** Representative immunoblot from cultures transfected as in A shows relatively equal expression of the WT, K40A, and K40Q α-tubulin-mCherry proteins. **(C)** Representative immunoblots for DRGs transfected with two different siRNAs targeting Miro1 mRNA (siMiro1) show specificity for both the anti-Miro1 and anti–Miro1-AcK105 antibodies used here. **(D)** Representative immunofluorescent images along axons of cultured DRG neurons show that signals for anti–Miro1-AcK105 antibody (FITC) are lost when immunizing Miro1-AcK105 peptide is included in immunostaining mixture. MitoTracker Green and NF (Cy5) signals are not appreciably affected. ImageJ was used for image cropping, pseudocoloring, and channel merging (scale bar = 20 µm; 100×/1.4 NA objective used).

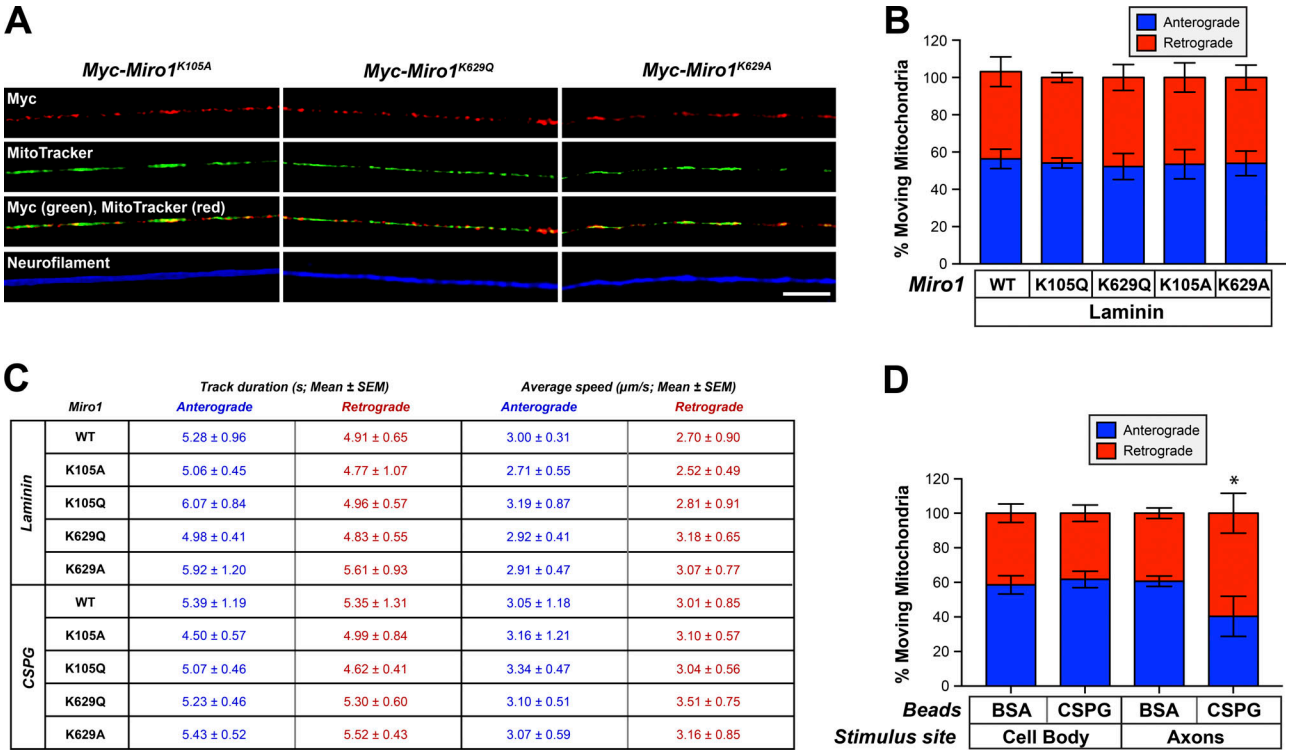

Figure S7. **Myc-Miro1 mutants localize to axonal mitochondria. (A)** Representative XY confocal images of axon shafts from DRG cultures expressing Myc-Miro1^{K1052A}, Myc-Miro1^{K629Q}, and Myc-Miro1^{K629A} are shown. Signals for Myc (FITC), MitoTracker Green, and NF (Cy5) are shown as indicated. The signals for anti-Myc antibodies show strong overlap with MitoTracker signals in these axons. See Fig. 7 E for corresponding images of Myc-Miro1 and Myc-Miro1^{K105Q} (scale bar = 10 µm; 100×/1.4 NA objective used). **(B)** Average distribution of anterogradely and retrogradely moving axonal mitochondria in DRG neurons grown on laminin and transfected with the indicated Miro1 mutants are shown ± SEM (blue = anterograde and red = retrograde for *n* = 20 axons over three culture preparations; there are no statistical differences by one-way ANOVA with pairwise comparison and Tukey post hoc). Distributions for neurons cultured on CSPG substrate is shown in Fig. 7 F. **(C)** Kinetics for axonal mitochondrial motility in DRG neurons cultured on laminin and expressing indicated Miro1 mutants are shown as average values ± SEM. Anterograde in blue and retrograde in red text. There are no statistical differences in track duration or average speeds of mitochondria by one-way ANOVA with pairwise comparison and Tukey post hoc (*n* = 20 axons over three culture preparations; see Fig. 7 F for mitochondrial motility on CSPG substrate). **(D)** Average distribution of anterogradely and retrogradely moving axonal mitochondria for DRG neurons where aggrecan-coated microspheres (CSPG-beads) were adjacent to axons versus cell body is shown ± SEM (see Fig. 7 G for responses with Miro1 mutants; *n* = 15 axons over three culture preparations; *, P ≤ 0.01 for CSPG-exposed vs. BSA-exposed axons by one-way ANOVA with pairwise comparison and Tukey post hoc).